Generalized Frequency Division Multiplexing for 5G Cellular Systems: A Tutorial Paper

Vitthal Lamani and **Dr. Prerana Gupta Poddar**
Department of Electronics and Communication Engineering, BMS College of Engineering, Bull Temple Road, Bangalore 560019 Karnataka, India
preranagp.ece@bmsce.ac.in

Abstract - **Fourth generation (4G) cellular systems have been optimized to provide high data rates and reliable coverage to mobile users in very dense areas. The next generation cellular systems will face much more diverse application requirements. We study a unified physical layer waveform Generalized Frequency Division Multiplexing (GFDM) to address these requirements. GFDM is a generalized and more bandwidth efficient form of the widely used orthogonal frequency division multiplexing (OFDM) modulation scheme. In this paper, we give detailed description of a prototype transceiver structure using GFDM. The performance of GFDM is analyzed for different digital modulation techniques over AWGN and Rayleigh fading channels. Channel equalization is performed with zero forcing (ZF) and minimum mean square error (MMSE) based equalizers. Comparison between GFDM and OFDM systems is presented.**

Keywords: Generalised Frequency Division Multiplexing, Orthogonal Frequency Division Multiplexing, Zero Forcing and Minimum Mean Square Equalizers

I. INTRODUCTION

MOBILE communication has become an essential tool for the modern society. 4G mobile systems which offer peak data rates up to 1 Gbps for low mobility users have seen extensive research and deployment over the last decade. The outline or model for future fifth generation (5G) networks have requirements that go beyond the high data rates of 4G [1][2]. The 5G networks have some envisaged scenarios like Tactile Internet, machine type communication (MTC), and Wireless Regional Area Network (WRAN) [3-5].

Orthogonal Frequency Division Multiplexing (OFDM) is a widely used PHY layer technique mainly because of its robustness to multipath channels (which becomes even more significant in MIMO) and easy implementation using Fast Fourier Transform (FFT) algorithms [6-8]. But OFDM has some significant limitations, when it comes to the application scenarios predicted for 5G networks. Machine-to-machine (M2M), MTC requires low power utilization, which makes the orthogonality between subcarriers too expensive, because strict synchronization process requires more power [2]. OFDM signals with one cyclic prefix (CP) per symbol would present a prohibitive low spectral efficiency. Applications like Tactile Internet and vehicle-to-vehicle (V2V) [9] require low latency; demand for short bursts of data cannot be provided efficiently by OFDM. Additionally, for opportunistic and dynamic spectrum access, a challenge is the high out-of-band (OOB) emission present in OFDM [11]. Because of all these challenges, OFDM is not the most promising waveform for the next generation networks. There is a lot of research going on for alternative multicarrier schemes that are candidates for the PHY layer of next generation mobile communication systems.

GFDM has recently received a great deal of attention because of its attractive properties. It is a generalized form of OFDM, which keeps most of the advantageous properties of OFDM while addressing its limitations [12]. Farhang *et al.* discuss [13] that the limitations due to the carrier aggregation in an OFDM system is eliminated by using GFDM system, since it provides a very low out-of-band radiation. Moreover, GFDM uses circular filtering instead of linear filtering used in OFDM, which eliminate the prototype filter transient intervals and hence the latency. Because of this, it can provide for low latency applications like internet of things (IoT) and M2M. It is also robust to loss of orthogonality and limits the inter-carrier interference (ICI), by filtering the subcarriers using a well-designed prototype filter.

This paper is tutorial in nature and aims to provide a basic understanding of GFDM as a candidate PHY layer technology for 5G systems. It also presents detailed performance results for GFDM with different modulation techniques, under different channel conditions and finally provides a comparison with an OFDM based communication system. This paper is organized as follows: section 1 introduces the deficient aspects of OFDM pertinent to the envisaged 5G systems and presents a literature survey on GFDM, section 2 describes in detail the system model of a GFDM based transceiver, section 3 discusses the performance results of GFDM and its comparison with an OFDM system, and finally section 4 concludes the paper. We use the following standard notation – matrix and vector quantities are written in bold fonts; superscripts ^{T} and ^{H} denote matrix transpose and Hermitian operations respectively.

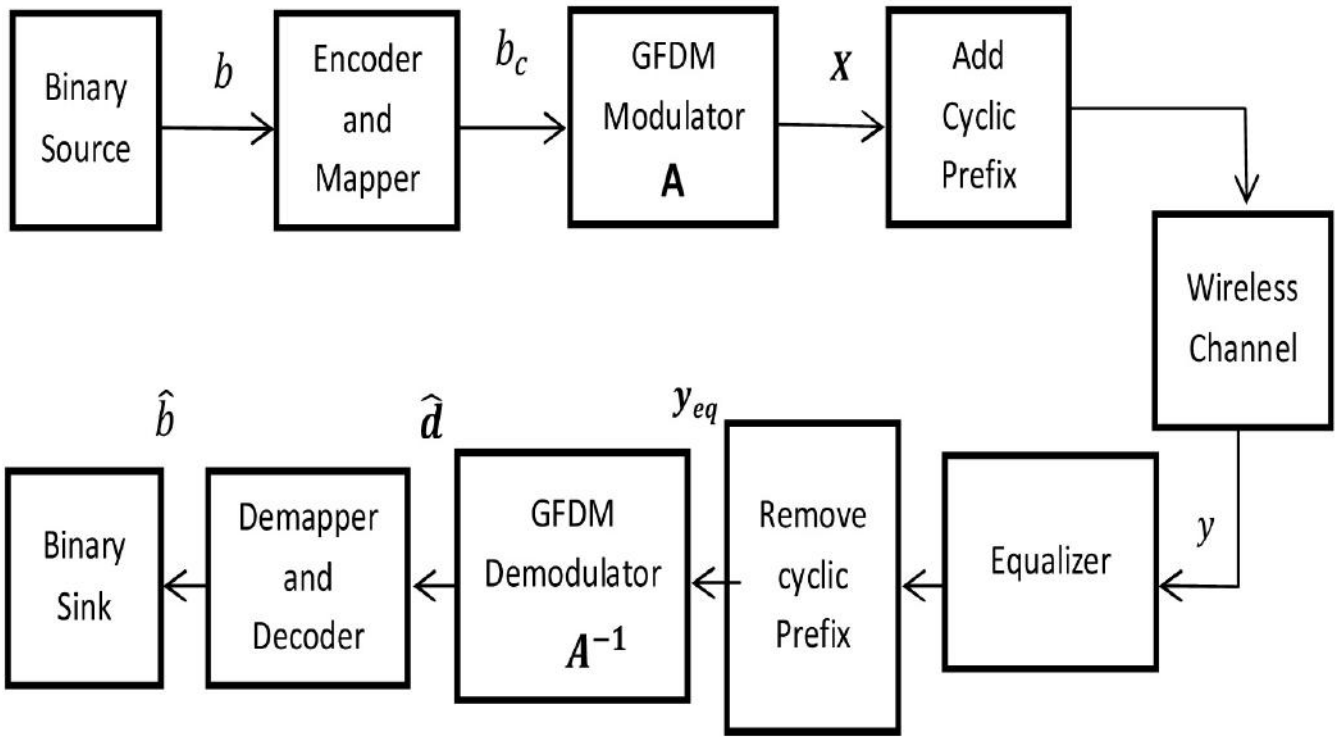

Figure 1. Block diagram of GFDM transceiver.

II. SYSTEM MODEL

The block diagram shown in Figure 1 is a GFDM based transceiver. The binary data source generates the binary data stream b, this is encoded and mapped using a suitable digital modulation technique (BPSK, QPSK, or QAM) to obtain encoded symbols b_c. The encoded symbols belong to a set of 2^{μ}-complex constellation points where μ denotes the number of bits per symbol, also known as order of modulation. The resulting symbols b_c are arranged as an input data vector, having K elements at a time, where $K = MN$ *i.e.* product of two integers. The K elements can be visualized as disintegrated into N subcarriers with M symbols in each GFDM data block. In a GFDM data block, M symbols overlap in time, therefore M is the GFDM system overlapping factor. The $NM \times 1$ column vector $\boldsymbol{d} = [\boldsymbol{d}_0^T \ldots\ldots\ldots\ldots \boldsymbol{d}_{N-1}^T]^T$ contains the complex data symbols of one GFDM block, where the $M \times 1$ data vector $d_i = [d_i(0) \ldots\ldots\ldots d_i(M-1)]^T$ denotes the data symbols to be transmitted on the subcarrier.

Figure 2 shows the organization of individual elements in one data block on a time frequency grid. Here B denotes available channel bandwidth (split as N subcarriers) and T is the time duration of one GFDM data block. As defined earlier, the element $d_n(m)$ denotes the information symbol sent on the n^{th} subcarrier and m^{th} symbol of the block. In figure 2, we can visualize the NM elements of vector $\boldsymbol{d}$ to be arranged in a grid. In this case, there are a total of 12 elements divided into $N = 4$ subcarriers and $M = 3$ sub-symbols.

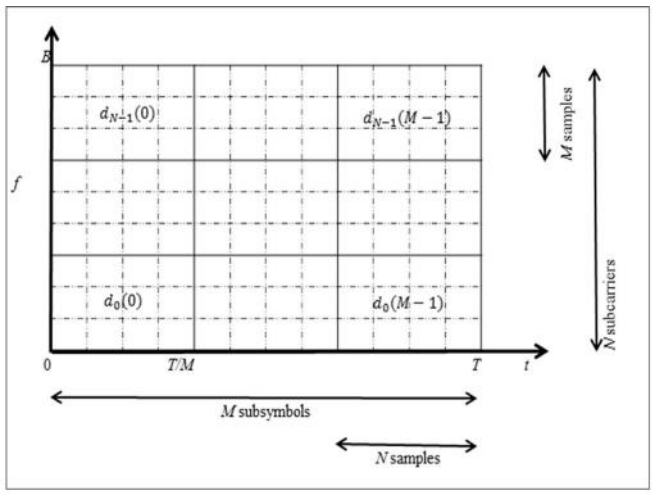

Figure 2. Partitioning in time and frequency.

The stepwise baseband operations of GFDM modulator block of Fig.1 are shown in Fig.3. This figure is partial replication of the block diagram in [13]. The GFDM modulator consists of serial to parallel converter to create vector, followed by up-sampler and prototype filter, where the shaping of transmit signal is done. Then all the signals are modulated to individual

subcarriers and summed up to form a complete GFDM signal. Cyclic prefix is added to reduce the impairments on the wireless channel.

This sequence of operations is now described in more detail. The data symbols to be transmitted on the subcarrier are first interpolated by a factor of *N* to form an impulse train, as given by

$$s_i(n) = \sum_{m=0}^{M-1} d_i(m)\,\delta(n - mN) \qquad n = 0, \ldots\ldots\ldots\ldots, NM-1 \tag{1}$$

Then these individual subcarriers

$$s_i = [s_i(0), \ldots\ldots\ldots\ldots\ldots\ldots\ldots s_i(NM\text{-}1)]^T$$

are convolved circularlywith the pulse shaping prototype filter.

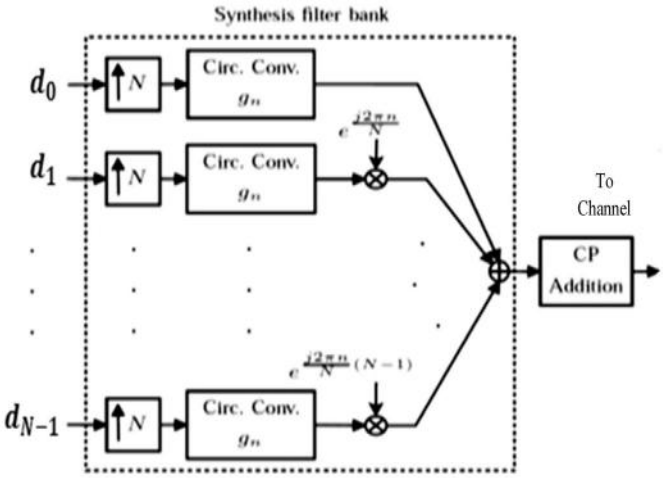

Figure 3. Baseband GFDM modulator.

Inter-symbol interference is controlled by shaping the transmission pulse with an appropriate pulse shaping filter like sinc filter, raised cosine filter, or Gaussian filter. We may observe from Figure 3, the distinguishing feature of GFDM from OFDM. The individual carriers are non-orthogonal in GFDM and pulse shaping and modulation is performed separately; contrary to OFDM, where the modulation / demodulation of all *N* subcarriers is performed by a single IFFT/FFT operation. Here we have used root raised cosine filter, the family of filter spectra that resembles Nyquist filter, as shown in eqn (2) and plotted in Figure 4.

$$p(t) = \frac{2\beta}{\pi\sqrt{T_s}}\left(\frac{\left(4\beta\frac{t}{T_s}\right)\cos\left[(1+\beta)\pi\frac{t}{T_s}\right] + \sin\left[(1-\beta)\pi\frac{t}{T_s}\right]}{\left(4\beta\frac{t}{T_s}\right)\left[1-\left(4\beta\frac{t}{T_s}\right)^2\right]}\right) \tag{2}$$

Here β is the roll-off factor and is a real number in the interval $0 \le \beta \le 1$, which controls the signal bandwidth. The frequency response of the root raised cosine filter has a unit gain at low frequencies, but in the middle frequencies, the response is square root of raised cosine function, at high frequencies it totally attenuated. We can observe from Fig.4 that as β increases, the width of the pulse decreases. For the special case of $\beta=0$, the response resembles a Nyquist filter *i.e.* sinc pulses in $(\pi t \mid \mathrm{Ts})/(\pi t \mid \mathrm{Ts})$ [14].

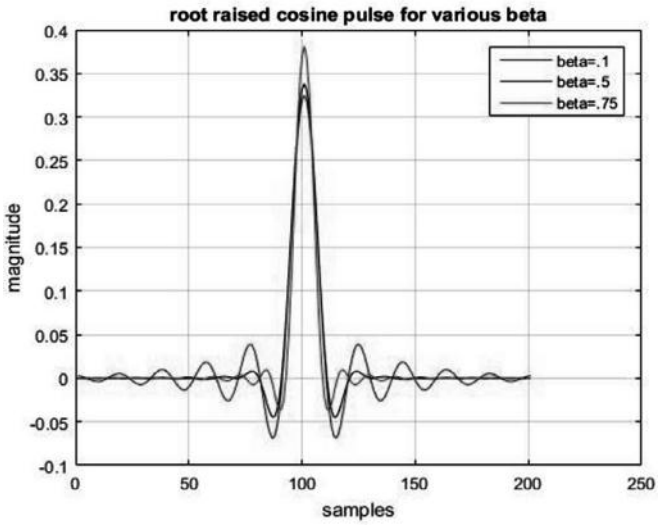

Figure 4. Raised cosine pulse for different values of β (roll off factor).

Let $g = [g_{(0,\ldots\ldots)}\, g_{(NM-1)}]^T$ be the $NM \times 1$ vector, containing the set of co-efficients of the prototype filter for pulse shaping. Note that zero padding is performed to maintain the size of *g* same as the length of data vector for one GFDM block. The same procedure is performed for each subcarrier branch, and the resulting signals are aggregated to form the GFDM signal *x*(n)

$$x(n) = \sum_{i=0}^{N-1}\sum_{m=0}^{M-1} d_i(m)\, g\{(n - mN)\ mod\ NM\} e^{\frac{j2\pi in}{N}},$$

$$n = 0, \ldots\ldots, NM-1$$

$d_i(m)$ is the complex data symbol. Effect of mod operator is the circular shift of pulse shaping filter co-efficient in time domain. The shifting operation in the frequency domain (up-conversion to subcarrier frequency) is done by the complex exponential multiplication *i.e.* $e^{(j2\pi in/N)}$. These two operations are at the heart of generalized frequency division multiplexing. Cyclic prefix is added tox *(n)*, *i.e.*

the *CP* symbols at the end of $x(n)$ are appended at the beginning, and the final length of one GFDM data block becomes $NM + CP$ symbols.

The whole operation can be compactly represented as the multiplication of data vector $\boldsymbol{d}$ of size $NM \times 1$ with a modulation matrix $\boldsymbol{A}$ of size $NM \times NM$ to form the complete GFDM signal as [13].

$$X = A \times d \tag{4}$$

We may observe that the NM entries of vector $\boldsymbol{X}$ are nothing but the values of $x(n)$, $n = 0, NM\text{-}1$ calculated in (3). All the signal processing steps involved in modulation as given by (3), are enclosed in the modulation matrix. The entries of matrix are given by.

$$[A]_{n,m} = g[(n - mN) \bmod NM]e^{\frac{-j2\pi nm}{NM}} \tag{5}$$

Some of the individual elements of $\boldsymbol{A}$ are found by solving (5) as follows:

For the first row, $n = 0$,

$$[A]_{0,0} = g_0$$
$$[A]_{0,1} = g_{\{-N \bmod MN\}}e^0 = g_{-N}$$
$$[A]_{0,2} = g_{\{-2N \bmod MN\}}e^0 = g_{-2N}$$
$$[A]_{0,(M-1)} = g_{\{(m-1)N \bmod MN\}}e^0 = g_{-(M-1)N}$$

For the second row,n=1,

$$[A]_{1,0} = g_{\{1 \bmod MN\}}e^0 = g_1$$

$$[A]_{1,1} = g_{\{(1-N)mod\ MN\}}e^{\frac{j2\pi}{NM}} = g_{(1-N)}e^{\frac{j2\pi}{NM}}$$

$$[A]_{1,(M-1)} = g_{\{(1-(M-1)N)mod\ MN\}}e^{\frac{j2\pi(M-1)}{NM}} = g_{(-1-N)}e^{\frac{j2\pi(M-1)}{NM}}$$

Similarly for $n = N - 1$,

$$[A]_{(N-1),0} = g_{\{(N-1-0)mod\ MN\}}e^0 = g_{N-1}$$

$$[A]_{(N-1),(M-1)} = g_{\{(N-1-(M-1)N)mod\ MN\}}e^{\frac{j2\pi(M-1)(N-1)}{NM}} = g_{1-2N}\,e^{\frac{j2\pi(M-1)(N-1)}{NM}} \tag{6}$$

and so on.

From the above calculations, the elements of modulation matrix A can be interpreted as follows: the first column of the matrix A has N co-efficients of pulse shaping filter with zero padding to make it $NM \times 1$. The subsequent columns are found by circularly shifting the first column, finally forming a matrix of order $NM \times NM$. For example, if $N = 4$, $M = 7$, the dimension of matrix is 28×28. Figure 5 shows the plot of values of matrix A, plotted vs. subcarrier index and symbol index, for a roll-off $\beta = 0.1$. From Figure 5, we observe that each pulse (black curve) represents a single carrier and group of four successive pulses of the same magnitude represents one symbol. The circulant nature of matrix A is also evident. If we compare figure 4 and 5, we find that figure 5 is nothing but the curve for $\beta = 0.1$ in Figure 4, along with a complex exponential scaling term, that is shifted in frequency and time over and over to give a contour plot.

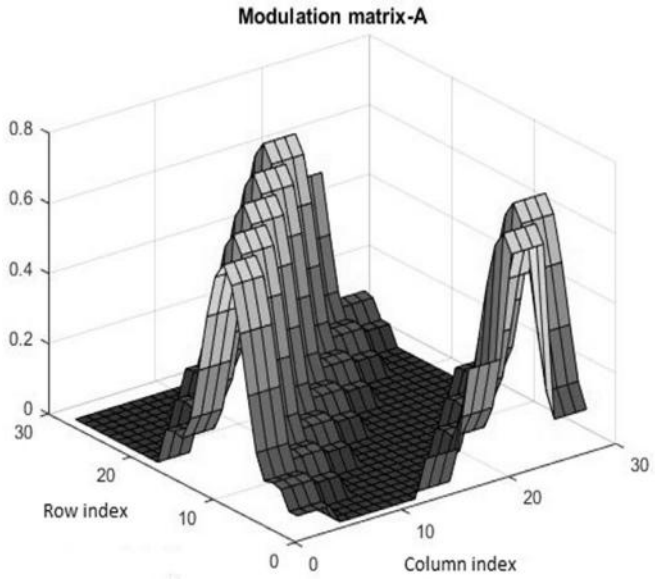

Figure 5. Modulation matrix for $N = 4$, $M = 7$.

Transmission through a wireless fading channel is modeled as

$$y(n) = hx(n) + w(n) \tag{7}$$

where $y(n)$ is the received counterpart of transmitted signal $x(n)$, at a discrete time instant n. Here h denotes the channel co-efficient. At the receiver side, the effect of fading channel can be eliminated by using suitable equalizer methods. The methods used in this work are zero forcing (ZF) and minimum mean-square error equalization (MMSE) [14].

For a general multiple input-multiple output (MIMO) system, having J transmit antennas and K receive antennas, and a $J \times K$ channel co-efficient matrix H, the response of ZF equalizer is given as $E_{ZF} = (H^H H)^{-1} H^H$. ZF equalization completely removes self-interference at the cost of enhancing the noise, it shows poor performance for smaller values of SNR. This can be improved by using MMSE equalization, whose response is $E_{MMSE} = (H^H H + \sigma^2 I_K)^{-1} H^H$. Here $\sigma^2 I_K$ denotes the covariance of noise and I_K is an identity matrix of size $K \times K$. In this work, single input single output (SISO) system is used *i.e.* $J=1$ and $K=1$, Hbecomes a single value channel co-efficient (= h from eqn. 7) and the identity matrix reduces to unity. H^H is the Hermitian of matrix H, for SISO system it reduces to H^H=c onjugate transpose $(H) = h^*$.

Once the received signal is equalized, the CP is removed and zero forcing receiver is used to recover the original transmitted complex data block. This is given by

$$d\hat{} = A^{-1} y_{eq} \qquad (8)$$

where y_{eq} the $NM \times 1$ size equalizer output matrix, corresponding to received signal vector y, y is the $NM \times 1$ received signal vector of $y(n)$ values of (7), when the index n is allowed to vary over 0 to NM -1, and A^{-1} is the $NM \times NM$ size inverse of modulation matrix A.

Once the zero forcing receiver reconstructs the complex data symbols, they are down sampled, and converted from parallel to serial. Then demapping and decoding is done to reverse the symbol mapping and encoding respectively, used at transmitting side. A comparison is made between the original data bits at the transmitter to find the error rate performance.

III. RESULTS AND DISCUSSION

The simulations in this work have been performed using MATLAB environment with system objects programming paradigm. This approach allows for dynamic system design and real time data processing. Figure 6 shows the BER performance of different baseband digital modulation techniques used with GFDM and transmitted over AWGN channel. The parameters used are: number of input samples per GFDM data block =2304, number of GFDM subcarriers $N = 64$, $M = 36$, RRC filter with roll-off factor $\beta = 0.1$, CP of length 16. We observe that at 10 dB SNR, QPSK has 10 dB better performance when compared to 16-QAM. Hence, QPSK-GFDM performs well and is more robust than QAM-GFDM.

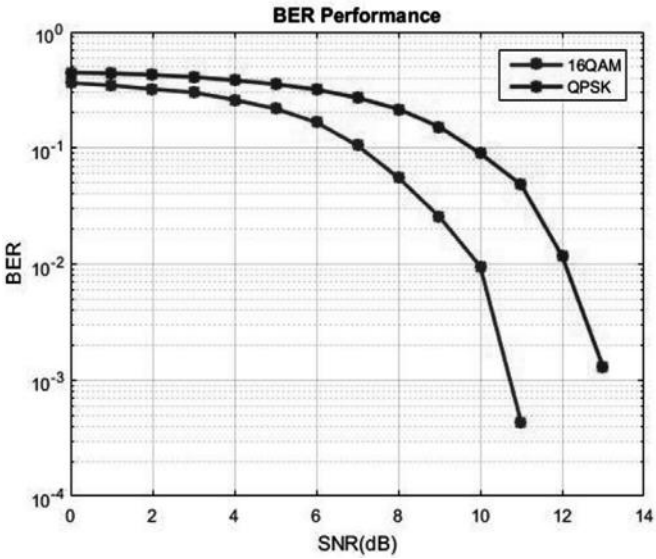

Figure 6. BER performance of GFDM over AWGN channel for different modulation schemes.

Figure 7 shows the BER performance of different baseband digital modulation techniques used in combination with GFDM over Rayleigh fading channel. The modulation schemes considered here are BPSK, M-ary PSK and M-ary QAM. We observe that 64-PSK as well as 16-PSK, with ZF equalization has very poor BER performance as compared to other systems. Both these results are seen to saturate at a BER above 0.1. As we may expect, in terms of BER, the MMSE equalizer always performs better than ZF equalizer. At an SNR 20dB, the MMSE-GFDM gives almost 7 dB better performance than ZFE-GFDM. Moreover, at an SNR of 18 dB, 16-QAM with MMSE equalization gives 10 dB better performance than 16-PSK ZF equalization.

This gain is achieved partly from the strength of MMSE over ZF, as explained earlier and partly from the fact that 16 PSK has 16 constellation points equally spaced on a unit circle, which allows smaller decision regions as compared to 16 QAM where the constellation points are arranged in a 4×4 square lattice. As we may expect, the BER curve for BPSK-MMSE equalization is better than all the other BER curves in Figure 7. With BPSK-GFDM-MMSE system, a BER less than 0.01 is achieved for SNR higher than 18 dB. We may observe that the BPSK-GFDM-ZF BER curve also closely follows the BPSK-GFDM-MMSE curve till SNR = 16 dB. However, as SNR increases, fading effect becomes more dominant compared to AWGN and the strength of MMSE compared to ZF becomes evident as the two curves separate out.

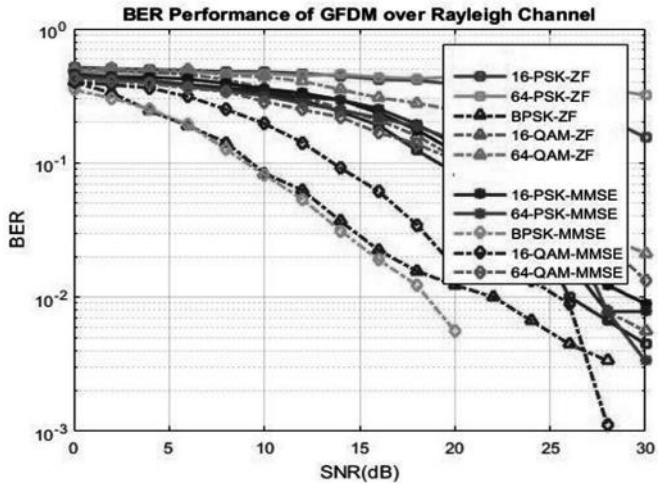

Figure 7. BER performance of GFDM over Rayleigh fading channel for different modulation schemes.

Figure 8 shows the symbol error rate (SER) performance of a 16-QAM-GFDM system using RRC filter with roll off factor $\beta = 0.1$, when transmitted over Rayleigh fading channel with ZF and MMSE equalization at the receiver. The pattern of results remains identical as in Fig 7; however for brevity, we have avoided plotting SER curves for all digital modulation schemes considered earlier. Our result in Figure 8 also matches the CP-GFDM plotted theoretically in Fig.8 (*b*) of reference [12]. From the plot in Fig.8, we observe that for SNR > 26 dB, an SER close to is achieved by 16-QAM-GFDM-MMSE.

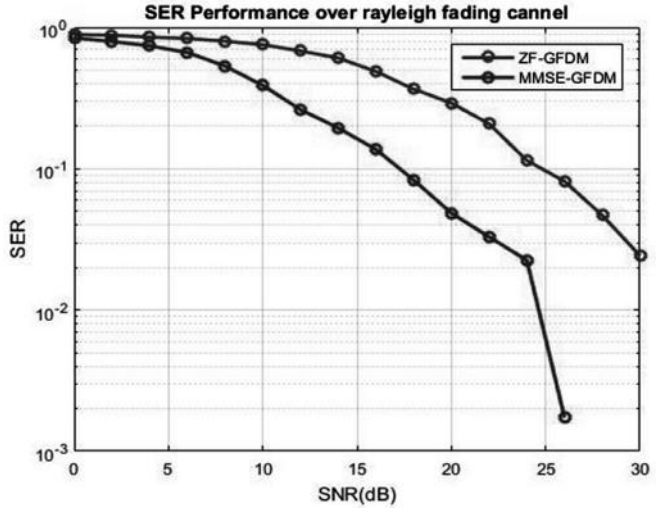

Figure 8. SER performance of 16-QAM GFDM over Rayleigh fading channel.

Figure 9 (*a*) and (*b*) show the comparison of bit error rate (BER) and symbol error rate (SER) performance of 16 QAM-GFDM and 16 QAM-OFDM systems with ZF and MMSE equalizers, when transmitting over Rayleigh fading channel. The complex baseband OFDM signal in time domain [6] is given as

$$x(t) = \frac{1}{N}\sum_{n=0}^{N-1} X_n\, e^{j2\pi\Delta f t} \quad , \; 0 \le t \le T \tag{9}$$

where T is the OFDM symbol duration, is the modulation symbol on each subcarrier, and is the subcarrier spacing. It may be observed that OFDM modulation is achieved through a single IFFT operation with N parallel subcarriers, and CP symbols are appended to the beginning of each OFDM symbol. It eliminates the need for individual subcarrier upsampling, filtering and processing as done in Figure 3.

Simulation parameters used for comparison are as follows: number of input samples 2304, IFFT size in OFDM is 128, number of sub-carriers in GFDM is also 128, single tap Rayleigh fading channel, CP length is 16 for one GFDM data block, in OFDM for each data symbol, it is 25% overhead with respect to data subcarrier length. As we can see from Fig 9 (*a*), GFDM-MMSE gives 7 to 10 dB better BER performance than GFDM-ZF.

The BER result for OFDM-ZF, shown as pink line in the legend is not visible because it coincides with the blue curve of GFDM-ZF. At low SNRs, the BER of OFDM-MMSE (green curve) coincides with OFDM-ZF, but as the SNR exceeds 10 dB, OFDM-MMSE shows consistent improvement and coincides with the performance of GFDM-MMSE. Thus 16-QAM-GFDM-MMSE as well as 16-QAM-OFDM-MMSE are able to achieve a BER of 0.001 for SNR > 25 dB on a Rayleigh fading channel. The SER curves of Figure 9 (*b*) also show an identical pattern of results as Figure 9 (*a*). In a nutshell, the GFDM system shows a performance which is identical to or better than the OFDM system.

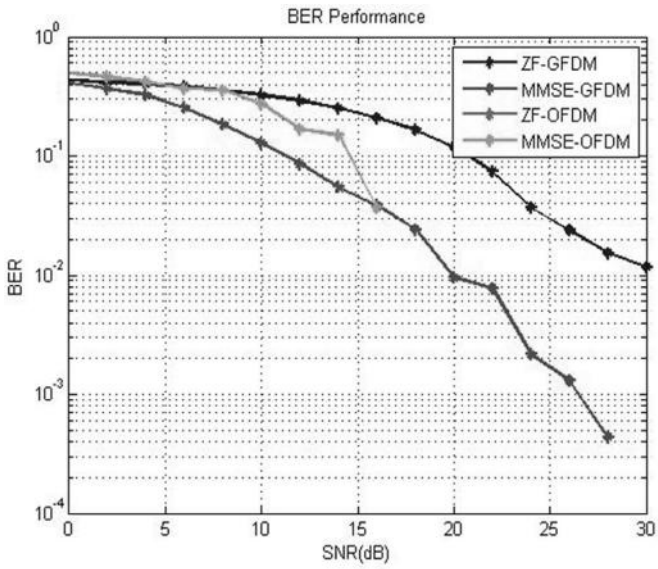

Figure 9. (*a*) BER and (*b*) SER performance comparison for GFDM and OFDM on Rayleigh fading channel.

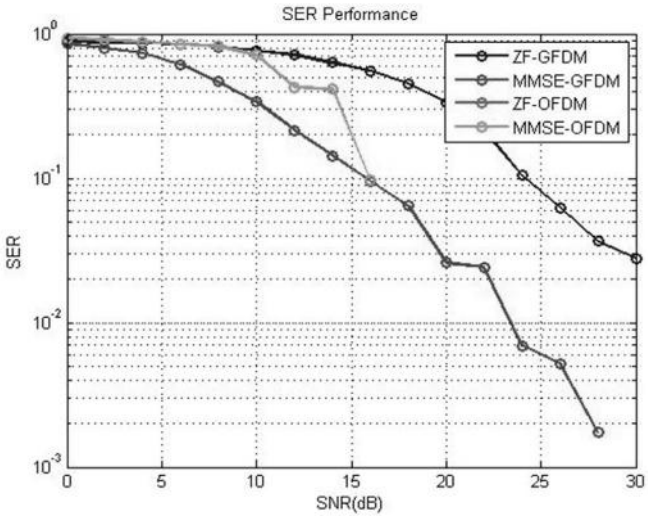

IV. CONCLUSION

In this paper, we analyze and implement the generalized frequency division multiplexing modulation technique, a strong candidate for the physical layer of future generation cellular communication systems. Apart from giving better BER and SER performance, the GFDM system addresses some drawbacks of the OFDM system, like reduced out-of-band emission by the circularly shaping the sub-carrier pulses. Numerous issues still need to be resolved, like higher computational complexity and delays as compared to OFDM because of the need for individual subcarrier processing in GFDM. However, our study delineates that GFDM has the capability to satisfy the necessities of the next generation mobile wireless systems.

V. REFERENCES

[1]. G. Fettweis and S. Alamouti, "5G: Personal Mobile Internet Beyond What Cellular Did to Telephony," *IEEE Communications Magazine*, Volume 52, Number 2, Feb. 2014, pp. 140–145.

[2]. G. Wunder, P. Jung, M. Kasparick *et al*. "5 G NOW: Non-Orthogonal, Asynchronous Waveforms for Future Mobile Applications," *IEEE Communications Magazine,* Volume 52 Number 2, Feb. 2014, pp. 97–105.

[3]. G. Fettweis, "The Tactile Internet: Applications and Challenges," *IEEE Vehicular Technology Magazine*, Volume 9, Number 1, Mar. 2014, pp. 64–70.

[4]. Y. Ding, Y. Jin, L. Ren and K. Hao, "An Intelligent Self-Organization Scheme for the Internet of Things," *IEEE Computational Intelligence Magazine*, Volume 8, Number 3, Aug. 2013, pp. 41–53.

[5]. N. Tadayon and S. Aissa, "Modeling and Analysis of Cognitive Radio Based IEEE 802.22 Wireless Regional Area Networks," *IEEE Trans. Wireless Communications*, Volume 12, Number 9, Sep. 2013, pp. 4363–4375.

[6]. J. Bingham, "Multicarrier Modulation for Data Transmission: An Idea Whose Time Has Come," *IEEE Communications Magazine*, Volume 28, Number 5, May 1990, pp. 5–14.

[7]. M. Mirahmadi, A. Al-Dweik and A. Shami, "BER Reduction of OFDM Based Broadband Communication Systems over Multipath Channels with Impulsive Noise," *IEEE Trans. Communications*, Volume 61, Number 11, Nov. 2013, pp. 4602–4615.

[8]. S. Fechtel and A. Blaickner, "Efficient FFT and Equalizer Implementation for OFDM Receivers," *IEEE Trans. Consumer Electronics*, Volume 45, Number 4, Nov. 1999, pp. 1104–1107.

.[9]. M. Nekovee, "Quantifying Performance Requirements of Vehicle-to-Vehicle Communication Protocols for Rear-End Collision Avoidance," *Proc. IEEE 69th Veh. Tech. Conf*., Volume 1. Barcelona, Spain, Apr. 2009, pp. 1–5.

[10]. H. Kim, J. Kim, S. Yang *et al*., "An Effective MIMO-OFDM System for IEEE 802.22 WRAN Channels," *IEEE Trans. Circuits and Systems II: Express Briefs*, Volume 55, Number 8, Aug. 2008, pp. 821–825.Volume 12, Number 9, Sep. 2008, pp. 609–611.

[11]. J. van de Beek and F. Berggren, "Out-of-Band Power Suppression in OFDM," *IEEE Communications Letters*, Volume 12, Number 9, Sep. 2008, pp. 609–611.

[12]. N. Michailow, M. Matthe, I. Gaspar *et al*., "Generalized Frequency Division Multiplexing for 5th Generation Cellular Networks," *IEEE Trans. Communications*, Volume 62, Number 9, 2014, pp. 3045–3061.

[13]. A. Farhang, N. Marchetti and L.E. Doyle, "Low complexity transceiver design for GFDM," in arXiv: 1501.02940, http://arxiv.org/abs/1501.02940, 2015, pp. 1–9.

[14]. J.G. Proakis, *"Digital Communications,"* 4th edn., McGraw-Hill Book Co Singapore, International Edition 2001.

Vitthal Lamani was born in Karnataka, India, and received his BE and M.Tech degrees from the Visvesvaraya Technological University, Belagavi, Karnataka in 2014 and 2016 respectively.
His interests lie in wireless communication, digital signal processing and embedded systems.

Dr. Prerana G Poddar was born in Delhi, India and received her B.Tech degree from Guru Gobind Singh Indraprastha University Delhi in 2003.
She received her PhD in 2008 at the Dept of EC Engineering, Indian Institute of Technology Roorkee. She has over seven years of teaching and research experience, and is currently working as Associate Professor at the Department of Electronics and Communication Engineering, BMS College of Engineering Bangalore.
Her research interests lie in signal processing and PHY layer design for communication systems.